

Virtual Pets: Animatable Animal Generation in 3D Scenes

Yen-Chi Cheng^{1,3} Chieh Hubert Lin² Chaoyang Wang³ Yash Kant^{3,4}
 Sergey Tulyakov³ Alexander Schwing¹ Liangyan Gui¹ Hsin-Ying Lee³
¹ UIUC ² UC Merced ³ Snap Research ⁴ University of Toronto

<https://yccyencheng.github.io/VirtualPets/>



Figure 1. **Virtual Pets**. Given a 3D scene, we can generate diverse 3D animal motion sequences that are environment-aware.

Abstract

Toward unlocking the potential of generative models in immersive 4D experiences, we introduce Virtual Pet, a novel pipeline to model realistic and diverse motions for target animal species within a 3D environment. To circumvent the limited availability of 3D motion data aligned with environmental geometry, we leverage monocular internet videos and extract deformable NeRF representations for the foreground and static NeRF representations for the background. For this, we develop a reconstruction strategy, encompassing species-level shared template learning and per-video fine-tuning. Utilizing the reconstructed data, we then train a conditional 3D motion model to learn the trajectory and articulation of foreground animals in the context of 3D backgrounds. We showcase the efficacy of our pipeline with comprehensive qualitative and quantitative evaluations using cat videos. We also demonstrate versatility across unseen cats and indoor environments, producing temporally coherent 4D outputs for enriched virtual experiences.

1. Introduction

Recent advances in 3D modeling have noticeably improved the quality of modeling the shape [9, 15, 39, 64], appear-

ance [7, 8, 33, 45, 47, 49, 55], and dynamics [30, 42, 43, 52, 61] for both objects and scenes. While these advances are pivotal, there also remains a noticeable gap in the vivacity and interactivity inherent in 3D modeling, crucial for a fully immersive experience. Constructing virtual characters and imbuing them with dynamic, lifelike motions based on their environmental context is pivotal in various domains, including movie production, AR/VR development, and game design. Currently, these creative workflows demand extensive efforts from skilled artists and 3D designers who meticulously craft each object and manually plan motions. This manual process renders resulting experiences costly, difficult to scale, and time-consuming. Moreover, the designed motions often encounter challenges in seamless transferability to new environments. In response to these challenges, we propose the development of an environment-aware generative model for 3D motion in a data-driven manner. In this work, we specifically focus on modeling **Virtual Pets**: synthesizing realistic 3D motion for an animal species within diverse 3D scenes.

Developing an environment-aware generative model for 3D motion is challenging due to the scarcity of 3D motion annotations paired with corresponding and detailed environment geometry. Manual collection of such data with modern motion capture equipment is impractical for indi-

viduals due to the associated time and cost. Additionally, transferring the motions between subjects is difficult, due to anatomic variations of subjects and distinct environment layouts during the capture. We, therefore, seek to distill the environment-conditioned motion information from more accessible monocular videos on the Internet, which encompass diverse activities in various environments. Nevertheless, the problem remains difficult for three primary reasons: (a) traditional structure from motion [50, 51] cannot handle deformable objects, (b) the motions lack transferability without specific remedies, and (c) the motion needs to respect both the anatomy of the subject and the layout of the environment without compromising diversity.

To address these challenges, our approach involves leveraging a collection of videos featuring the target animal species. Our objective is to jointly reconstruct the articulated 3D shape of all foreground objects and to train an environment-aware generative model to produce realistic 3D motions within arbitrary 3D scenes. First, we extract 3D shape, motion, and affordance from a collection of videos. We adopt a deformable NeRF reconstruction method [61] to learn a species-level shared template for the foreground object on all videos. Subsequently, we fine-tune the instance-level deformable NeRF on each video, while the background is jointly reconstructed with a static NeRF, making sure the articulated motion is compatible with the background. With the reconstructed deformable foregrounds and static backgrounds, we train a conditional 3D motion generation framework to model the trajectory and articulation of the foreground object. During inference, the model can generate conditional 3D motion sequences given a foreground object and background information, rendering them into coherent videos. For textureless foreground or background, we adopt an off-the-shelf texturing method [6, 7] to produce a realistic and diverse appearance. In this work, we select *cats* as our target species due to their rich deformation in structure and appearance, diverse affordance, and the availability of sufficient video data.

We conduct extensive experiments on a collection of cat videos to demonstrate the effectiveness and efficacy of the proposed pipeline. We show that the proposed method performs favorably against the baseline methods, both quantitatively and qualitatively. Furthermore, we demonstrate our trained model generalizes to unseen cats and indoor room environments, generating temporally coherent 4D outputs [1](#).

2. Related Work

Dynamic reconstruction from videos. The emergence of Neural Radiance Fields (NeRF) [38] enabled promising progress in 3D reconstruction from multi-view images. Compared to images, reconstructing dynamics from videos poses significant challenges in handling time-varying dy-

namic content. Methods based on dynamic radiance fields either require multiple synchronized input videos [3, 30, 54, 65], or fail to handle complex dynamic scenarios [32, 42, 43, 57]. A stream of work [56, 58–61] focuses on reconstructing articulated objects from videos, as the prior shape knowledge is known and videos provide more signals to disentangle motion and morphology. In this work, we adopt RAC [61] as our backbone reconstruction method.

4D Generation. Compared to 2D and 3D data, 4D data is extremely difficult to collect, making it difficult to learn a 4D generative model in a data-driven manner, let alone the environment-aware conditioning that we are interested in. Recent successes in 3D generation [8, 33, 45, 47, 55, 69] distill knowledge from pretrained large-scale 2D diffusion models. Therefore, there are some recent efforts that follow the successes and extend the techniques to 4D [24, 52]. However, the quality is not satisfactory and it is difficult to enable additional control and manipulation. To bypass the current limitation and focus on the early exploration of the environment-aware 4D generation field, we target a category-specific setting and leverage the state-of-the-art animatable object reconstruction method [61] to provide training data necessary for the proposed pipeline.

Affordance Prediction. Affordance refers to the potential actions or interactions that an object or environment offers. Early efforts in 2D affordance prediction from images formulate the task as a categorical classification problem [5, 19, 41] or a heatmap regression problem [11, 22, 34, 40]. 3D affordance prediction is employed to understand human-scene interactions by predicting 3D locations and poses based on 2D images [12, 17, 31, 63, 67] or 3D scenes [18, 21, 66, 68]. In this work, given a 3D scene, we not only want to infer the potential 3D affordance, but also model the plausible movements in a generative manner.

Motion Prediction. Motion prediction has been studied, especially for human motion, using various backbone architectures from early Markov models [28], recurrent models [13, 23, 37], generative adversarial networks [4, 27], to the recent diffusion models [53]. The prediction can be conditioned on action class [16, 44], audio [27, 29], and text [2, 53]. However, most existing motion prediction methods are based on skeletons, disregarding surface geometry and appearance.

3. Method

In the following, we first describe how to extract shape, motion, and affordance from an unstructured monocular video collection (see Sec. 3.1). We then discuss our environment-aware generative model for 3D motion (see Sec. 3.2).

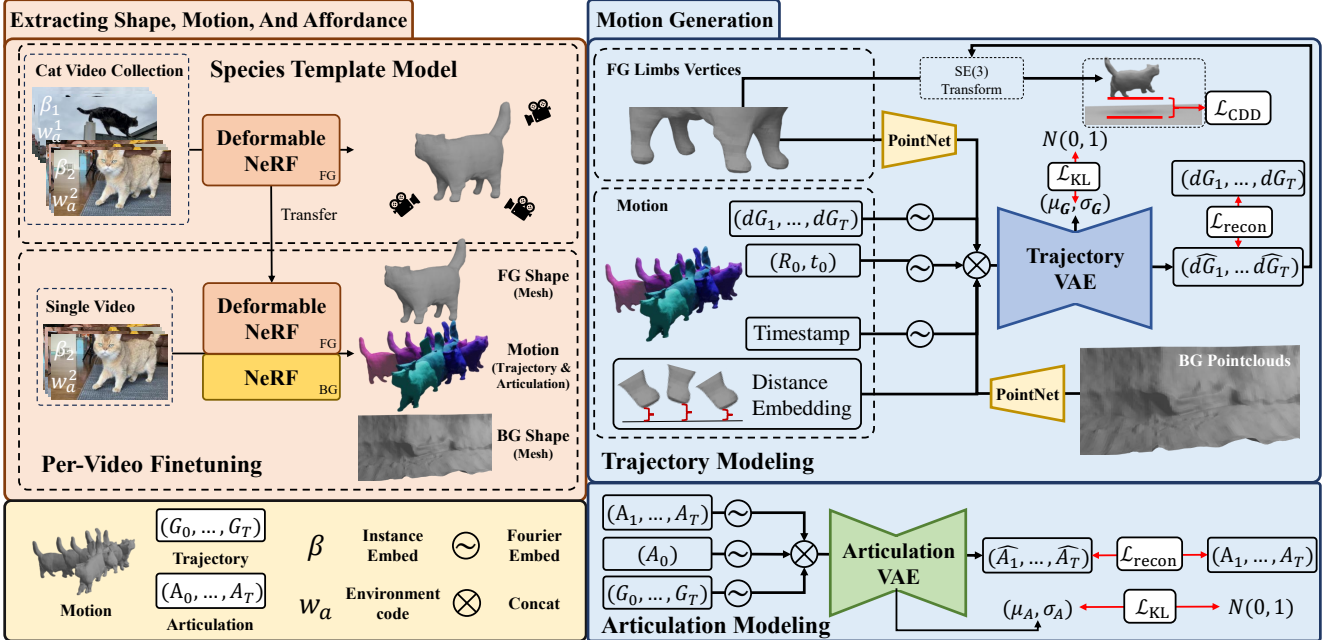


Figure 2. **The proposed framework of Virtual Pets.** To extract 3D shapes and motions from monocular videos: we first learn a *Species Articulated Template Model* with an articulated NeRF [61] using a collection of cat videos. We then perform *Per-Video Fine-tuning*. For each video, we further reconstruct the background with a static NeRF [38]. The articulated NeRF trained in the species-level stage is loaded and fine-tuned in this stage to make sure the motions, which are Trajectory and Articulation, respect the reconstructed background shape. After that, we train an environment-aware 3D motion generator with a *Trajectory VAE* and an *Articulation VAE*. It generates 3D motions based on vertices of the foreground limbs, distance from foreground to background, and pointclouds sampled from the background.

3.1. Extracting Shape, Motion, And Affordance Using Articulated 3D Reconstruction

Overview. To develop an environment-aware generative model for 3D motion, we extract the relevant representations from an unstructured monocular video collection in two stages, as illustrated in the left column of Fig. 2. In the first stage (see Sec. 3.1.1 for more), we focus on learning a species-level articulated template shape. This template shape serves as a foundational element, allowing subsequent alignment of motions extracted per video in the following stage. This alignment process significantly aids in the training of the generative model. Then, in the second stage (see Sec. 3.1.2 for more), we transfer and fine-tune the template shape on a per-video basis to obtain a more accurate object shape H_{fg} , trajectory $\{G_t\}$, and articulations $\{A_t\}$, where t denotes the time in the given video. Alongside fine-tuning the template shape, we simultaneously learn the background scene shape H_{bg} by learning a static NeRF model. The affordances of the objects in the environment can then be represented as interactions between the salient object shape H_{fg} and the background scene shape H_{bg} . This two-stage procedure enables to extract paired 3D motion and environment models from monocular videos.

3.1.1 Species Articulated Template Shape

Given videos of one animal species (in our case, cats), we learn a shared template shape. We represent the shared template shape via (c^t, d, G_t, A_t) , encompassing the color c^t , the signed distance function (SDF) value d , the object pose G_t , and the articulation A_t of the shape. The object pose $G_t = (R_t, s_t) \in SE(3)$ describes the object pose in the camera space, where rotation R_t and translation s_t transform the object from its rest pose in canonical space to the pose in camera space. We use a sequence of object poses $\mathbf{G} = [G_0, G_1, \dots, G_T]$ to characterize the global movements of the foreground object in the environment. Articulation $A_t \in \mathbb{R}^{3 \times B}$ expresses the local changes of B skeleton joints that deform the template model at every time step. To encapsulate all the global-local time-dependent spatial dynamics of the shape, we represent motion as “ $M_t = (G_t, A_t)$ ”.

To model the template shape, we use an implicit function F_θ , concretely, an articulated NeRF [61]. Given any 3d point \mathbf{x} in space \mathbb{R}^3 , for any time t , for any instance embedding $\beta \in \mathbb{R}^{128}$, and for any scene-dependent environment feature w_a , the implicit function returns the template shape (c^t, d, G_t, A_t) :

$$(c^t, d, G_t, A_t) = F_\theta(\mathbf{x}, \beta, w_a). \quad (1)$$

Both β and w_a are trainable parameters to learn the video-specific appearance such as the identity of the subject and the lighting condition of the environment.

F_θ is implemented with a combination of a skeleton, skinning weights W driven by the skeleton, and multiple Multi-Layer Perceptrons (MLPs) representing the shape and appearance deformed by the skinning weights. In the following, we describe the three components of the implicit function F_θ .

Shape and appearance. We encode canonical coordinate $\mathbf{x} \in \mathbb{R}^3$, viewing direction \mathbf{v}^t , instance embedding $\beta \in \mathbb{R}^{128}$, and environment embedding w_a into color c^t and SDF value d via an MLP, *i.e.*,

$$c^t = \text{MLP}_c(\mathbf{x}, \mathbf{v}^t, w_a), \quad (2)$$

$$d = \text{MLP}_{\text{SDF}}(\mathbf{x}), \quad \sigma = \Gamma(d), \quad (3)$$

where Γ is the CDF of a Laplacian distribution following the design of VolSDF [62].

Articulation. The articulation A_t is conditioned on instance embedding β , and is learned by modeling the joints $J_\alpha \in \mathbb{R}^{3 \times B}$ and skinning weights W_β for each video. The intuition of articulated 3D reconstruction is to derive a skeleton along with skinning weights, so that the sparse set of transition vectors (*i.e.*, articulation) applied on the skeleton joints can be converted into a dense motion field specifying the deformation of any point in the space over time. Following RAC [61], we define the skeleton topology of the template shape as a collection of $(B + 1)$ bones connected by B joints. The dynamics of the bones are determined by two learnable per-video embeddings: (1) the instance embedding β and (2) the location of the bone. We model the location of the joints via

$$J = \text{MLP}_J(\beta) \in \mathbb{R}^{3 \times B}, \quad (4)$$

encapsulating the movements of the bones. The skinning weights $W \in \mathbb{R}^{B+1}$ then specify the deformation factors of a canonical coordinate depending on the changes of all bones via

$$W = \sigma_{\text{softmax}}(d_\sigma(\mathbf{x}, \beta) + \text{MLP}_W(\mathbf{x}, \beta)). \quad (5)$$

Here, $d_\sigma(\mathbf{x}, \beta, \theta)$ is the Mahalanobis distance between the 3D point \mathbf{x} and the bones, following the design of BANMo [60]. Finally, we obtain the articulation A_t with

$$A_t = \text{MLP}_A(\beta, t) \in \mathbb{R}^{3 \times B}, \quad (6)$$

which represents the deformations of each bone. The articulation at each time step can be converted into a dense warp field D using dual quaternion blend skinning (QBS) [25, 61]. We denote this time-dependent dense warp field as

$$D_t = \text{QBS}(J, W, A_t, F_\theta). \quad (7)$$

Object Pose. The object pose G_t is computed by querying a time-conditioned MLP. It computes (R_t, s_t) to transform from an object’s rest pose in canonical space to the observed

object pose in the camera space via

$$G_t = \text{MLP}_{\text{pose}}(t). \quad (8)$$

Rendering and reconstructing. We can now perform volume rendering to render the images for NeRF training given (G_t, A_t) . Since the shape and appearance is modeled in canonical space, we first use G_t to transform the observed points to camera space. At time t , let $x_c^t \in \mathbb{R}^2$ refer to an observed pixel in camera space. $\mathbf{x}_c^t \in \mathbb{R}^3$ is a 3D point sampled along the ray starting at the camera center and passing through x_c^t . Using the object pose G_t^{-1} , we transform \mathbf{x}_c^t back to a point \mathbf{x} . We then use the articulation A_t to compute the dense warp field D_t using Eq. (7) to warp \mathbf{x} and query the MLP to obtain (σ, c^t) by querying $D_t(\mathbf{x})$ using MLP_c and MLP_{SDF} with Eq. (2) and Eq. (3). We can then perform volume rendering with (σ, c^t) following a conventional NeRF.

3.1.2 Per-video finetuning

Given a monocular video, we aim to reconstruct both the foreground mesh H_{fg} and the background mesh H_{bg} . To make sure the reconstructed mesh H_{fg} is compatible with mesh H_{bg} , we optimize the Deformable NeRF F_θ , initialized with the optimized F_θ in the articulated template learning stage, and background NeRF F_ϕ simultaneously. Specifically, given a 3D point \mathbf{x} and viewing direction v , we optimize foreground and background NeRFs for each video to reconstruct the full scene:

$$(d, c^t)_{\text{bg}} = F_\phi(\mathbf{x}, v), \quad (d, c^t)_{\text{fg}} = F_\theta(\mathbf{x}, \beta, w_a), \quad (9)$$

where σ is the density and c^t is the color at time t for 3D location \mathbf{x} . The final rendering after aggregation is determined by the depths estimated with σ .

After the species-level template shape learning and the per-video foreground and background joint optimization, we can extract the 3D motion $M_t = (G_t, A_t)$, foreground mesh H_{fg} , and background mesh H_{bg} with F_θ and F_ϕ given each video. The mesh for foreground and background is obtained by querying F_θ and F_ϕ to get the SDF in the canonical space, and by using a marching cube [35] to extract the shape at a level-set equalling 0. Pose G_t is obtained via Eq. (8), and articulation A_t is computed with Eq. (6).

3.2. Approach: Motion Generation

Given the extracted foreground mesh H_{fg} , the background mesh H_{bg} , and the motion M_t , our goal is to learn a conditional 3D motion generative model that can synthesize a 3D motion sequence of a cat in an indoor scene. We formulate the 4D generation in two stages. In the first stage (Sec. 3.2.1), we generate the 3D motion trajectory given a cat (*i.e.*, foreground mesh) and a scene (*i.e.*, background mesh) using a ‘Trajectory VAE’. Then, given the trajectory, we predict the corresponding articulation using an ‘Ar-

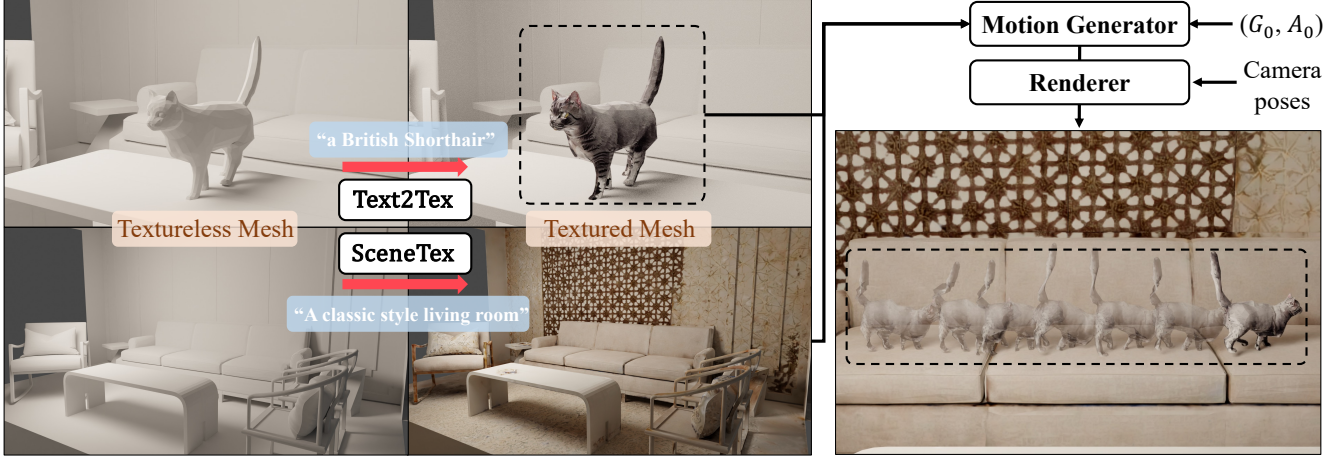


Figure 3. **Texturing and Rendering.** At inference time, given textureless foreground and background meshes, we first adopt Text2Tex [7] and SceneTex [6] to texture the meshes. Meanwhile, we generate the motion sequence using the trained trajectory VAE and articulation VAE. We then obtain the final predicted foreground mesh after deformation and transformation. Finally, the 3D motion sequences and the 3D scene are rendered to videos.

tication VAE’. The right column of Fig. 2 provides an overview of the proposed ‘Trajectory VAE’ and the ‘Articulation VAE’ for motion generation. In the second stage, as the foreground and background meshes are textureless, we adopt an off-the-shelf text-to-image diffusion model and score distillation sampling to perform texturing. Finally, we use the motion generated by our motion model to transform and deform the textured cat mesh for each timestep and render the 4D output into a video (Sec. 3.2.2). Fig. 3 shows the overall inference pipeline given foreground and background meshes, including texturing and rendering.

3.2.1 Learning Environment-Aware 3D Motion

Given a foreground mesh H_{fg} and a background mesh H_{bg} , we leverage a conditional VAE to generate the 3D motion $(\mathbf{G}, \mathbf{A}) = ((G_0, A_0), (G_2, A_2), \dots, (G_T, A_T))$. We generate the motion with two conditional VAEs – the Trajectory VAE (VAE_G) and the Articulation VAE (VAE_A). VAE_G first generates an environment-aware trajectory \mathbf{G} . Subsequently, the Articulation VAE (VAE_A) takes the trajectory as input to generate the corresponding articulation \mathbf{A} .

Trajectory VAE. Given the starting pose $G_0 = (R_0, s_0)$, we first generate the global trajectory $d\mathbf{G} = (dG_1, dG_2, \dots, dG_T)$, where dG_t is the relative rotation and translation at time t . Note, R_0, s_0 serve as the reference pose. For environment-awareness we additionally condition on (1) the vertices of the foreground limbs $\mathbf{P}_{limb} \in \mathbb{R}^{N_{fg} \times 3}$ (N_{fg} is number of vertices to sample from H_{fg}), (2) the distance $D_{fg} \in \mathbb{R}$ of the center of the foreground mesh to the background mesh H_{bg} , and (3) a pointcloud $\mathbf{P}_{bg} \in \mathbb{R}^{N_{bg} \times 3}$ sampled from H_{bg} . We use the PointNet [46] encoder to encode \mathbf{P}_{limb} and \mathbf{P}_{bg} .

Formally, our Trajectory VAE encoder first computes

embeddings of the pointcloud data via

$$\mathbf{z}_{bg} = \text{PointNet}(\mathbf{P}_{bg}), \quad \mathbf{z}_{limb} = \text{PointNet}(\mathbf{P}_{limb}). \quad (10)$$

We also embed the starting pose G_0 and the trajectory sequence extracted from video data via MLPs, i.e.,

$$\begin{aligned} \mathbf{z}_{G_0} &= \text{MLP}_G(G_0), \\ \mathbf{z}_{d\mathbf{G}} &= \text{MLP}_{d\mathbf{G}}(dG_1, dG_2, \dots, dG_T). \end{aligned} \quad (11)$$

Here, $\text{MLP}_{d\mathbf{G}}$ is an encoder implemented via an MLP to encode the features of the sequence $(dG_t)_{t=1}^T, dG_t \in SE(3)$. A latent variable encoding the trajectory is sampled from the normal distribution with mean and standard deviation obtained from an encoder \mathbf{E}_G implemented with a ConvNet and an MLP:

$$\mu_G, \sigma_G = \mathbf{E}_G(\mathbf{z}_{d\mathbf{G}}, \mathbf{z}_{G_0}, \mathbf{z}_{limb}, \mathbf{z}_{bg}, D_{fg}, \tau), \quad (12)$$

where $\mathbf{z}_G \sim N(\mu_G, \sigma_G)$. We use the decoder to generate a trajectory:

$$\hat{d\mathbf{G}} = \mathbf{D}_G(\mathbf{z}_G, \mathbf{z}_{G_0}, \mathbf{z}_{fg}, \mathbf{z}_{bg}, \tau), \quad (13)$$

where $\tau = (\tau_0, \tau_1, \dots, \tau_T) \in \mathbb{R}^{T \times 128}$ is a sequence of time-embeddings to enhance the temporal awareness. Note, we use the Fourier embeddings of $G_0, d\mathbf{G}$, and τ for better reconstruction results.

Articulation VAE. Given the trajectory \mathbf{G} and the starting articulation A_0 , VAE_A generates the corresponding articulation sequence \mathbf{A} . For each motion sequence, we first encode the trajectory \mathbf{G} and \mathbf{A} into latent codes

$$\begin{aligned} (\mathbf{z}_{G_0}, \mathbf{z}_{G_1}, \dots, \mathbf{z}_{G_T}) &= \text{MLP}_G(G_0, G_1, \dots, G_T), \\ \mathbf{z}_A &= \mathbf{E}_A(A_1, A_2, \dots, A_T), \\ \mathbf{z}_{A_0} &= \text{MLP}_A(A_0). \end{aligned} \quad (14)$$

Here, MLP_G is an MLP to encode the trajectory $(G_t)_{t=0}^T$. We also embed the starting articulation A_0 with MLP_A .

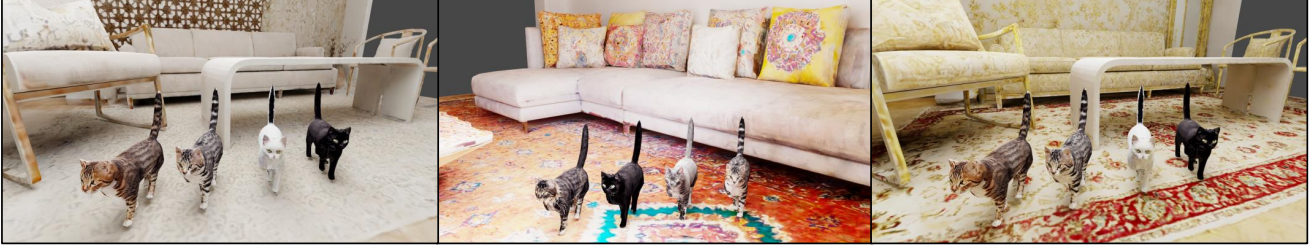


Figure 4. **Diverse textures.** We adopt Text2Tex [7] and SceneTex [6] to perform diverse texturing to both foreground objects and background scenes.

The means and standard deviations are obtained via:

$$\mu_{\mathbf{A}}, \sigma_{\mathbf{A}} = \mathbf{E}_{\mathbf{A}} \left((\mathbf{z}_{G_t})_{t=0}^T, \mathbf{z}_{\mathbf{A}}, \mathbf{z}_{A_0}, \tau \right), \quad (15)$$

where $\mathbf{E}_{\mathbf{A}}$ is an encoder implemented with a ConvNet and MLPs. We then sample a latent variable $\mathbf{z}_{\mathbf{A}} \sim N(\mu_{\mathbf{A}}, \sigma_{\mathbf{A}})$ that encodes the articulations from the normal distribution, and decode the articulation:

$$\hat{\mathbf{A}} = \mathbf{D}_{\mathbf{A}}(\mathbf{z}_{\mathbf{A}}, \mathbf{z}_{A_0}, \mathbf{z}_{\mathbf{G}}, \tau). \quad (16)$$

Training, Loss, and Inference. We train the model with a standard VAE objective: reconstruction loss and KL-divergence loss. Hence, training of $\text{VAE}_{\mathbf{G}}$ and $\text{VAE}_{\mathbf{A}}$ optimizes the ELBO, i.e.,

$$\begin{aligned} \mathcal{L}_{\text{VAE}_{\mathbf{G}}} &= \mathbb{E}_{q(\mathbf{z}_{\mathbf{G}}|\mathbf{G}, \mathbf{c}_{\mathbf{G}})} \log p(\mathbf{G}|\mathbf{z}_{\mathbf{G}}, \mathbf{c}_{\mathbf{G}}) \\ &\quad - \lambda_{\mathbf{G}}^{\text{KL}} D_{\text{KL}}(q(\mathbf{z}_{\mathbf{G}}|\mathbf{G}, \mathbf{c}_{\mathbf{G}}) || p(\mathbf{z}_{\mathbf{G}}|\mathbf{c}_{\mathbf{G}})), \end{aligned} \quad (17)$$

$$\begin{aligned} \mathcal{L}_{\text{VAE}_{\mathbf{A}}} &= \mathbb{E}_{q(\mathbf{z}_{\mathbf{A}}|\mathbf{A}, \mathbf{c}_{\mathbf{A}})} \log p(\mathbf{A}|\mathbf{z}_{\mathbf{A}}, \mathbf{c}_{\mathbf{A}}) \\ &\quad - \lambda_{\mathbf{A}}^{\text{KL}} D_{\text{KL}}(q(\mathbf{z}_{\mathbf{A}}|\mathbf{A}, \mathbf{c}_{\mathbf{A}}) || p(\mathbf{z}_{\mathbf{A}}|\mathbf{c}_{\mathbf{A}})). \end{aligned} \quad (18)$$

Here, $\mathbf{c}_{\mathbf{G}}$ and $\mathbf{c}_{\mathbf{A}}$ are the conditioned inputs for both VAEs. $\lambda_{\mathbf{G}}^{\text{KL}}, \lambda_{\mathbf{A}}^{\text{KL}}$ are the weights for the KL-divergence loss.

To reduce the floating phenomenon, where foreground objects are unnaturally detached from the ground, we add a ‘Floating Loss’ \mathcal{L}_{CDD} while training $\text{VAE}_{\mathbf{G}}$. Given the foreground limb vertices \mathbf{P}_{limb} , we transform it with ground-truth trajectory \mathbf{G}_{GT} and predicted trajectory \mathbf{G}_{pred} :

$$\begin{aligned} \mathbf{G}_{\text{GT}} \mathbf{P}_{\text{limb}} &= [G_0^{\text{GT}} \mathbf{P}_{\text{limb}}, G_1^{\text{GT}} \mathbf{P}_{\text{limb}}, \dots, G_T^{\text{GT}} \mathbf{P}_{\text{limb}}], \\ \mathbf{G}_{\text{pred}} \mathbf{P}_{\text{limb}} &= [G_0^{\text{pred}} \mathbf{P}_{\text{limb}}, G_1^{\text{pred}} \mathbf{P}_{\text{limb}}, \dots, G_T^{\text{pred}} \mathbf{P}_{\text{limb}}]. \end{aligned} \quad (19)$$

We then compute the Chamfer Distance between (1) the transformed vertices at each timestep and (2) background pointcloud \mathbf{P}_{bg} . Formally,

$$\begin{aligned} \mathcal{L}_{\text{CDD}} &= \frac{1}{T} \sum_{t=0}^T \left\| \text{Chamfer}(G_t^{\text{GT}} \mathbf{P}_{\text{limb}}, \mathbf{P}_{\text{bg}}) \right. \\ &\quad \left. - \text{Chamfer}(G_t^{\text{pred}} \mathbf{P}_{\text{limb}}, \mathbf{P}_{\text{bg}}) \right\|_1. \end{aligned} \quad (20)$$

Notice that we compute the distance between the ground-truth and predicted Chamfer Distance instead of directly using $(G_t^{\text{pred}} \mathbf{P}_{\text{limb}}, \mathbf{P}_{\text{bg}})$ in the objective. Solely minimizing the Chamfer Distance between vertices and background

will jeopardize motions like jumping.

In summary, the final objective is:

$$\mathcal{L} = \mathcal{L}_{\text{VAE}_{\mathbf{G}}} + \lambda_{\text{CDD}} \mathcal{L}_{\text{CDD}} + \mathcal{L}_{\text{VAE}_{\mathbf{A}}}. \quad (21)$$

3.2.2 4D Generation and Video Rendering

Given foreground mesh H_{fg} and background mesh H_{bg} without textures, we first adopt an off-the-shelf 3D texturing method Text2Tex [7], to obtain the textured UV-map for both foreground and background meshes. Then, we generate the motion sequence (\mathbf{G}, \mathbf{A}) . Users can specify the starting position and pose for the foreground mesh with $G_0 = (R_0, s_0)$. We then use $\text{VAE}_{\mathbf{G}}$ and $\text{VAE}_{\mathbf{A}}$ to generate the motion sequence $(\mathbf{G}^{\text{gen}}, \mathbf{A}^{\text{gen}})$. With \mathbf{A}^{gen} , we can adopt Eq. (7) to compute the warping field to deform the vertices of H_{fg} . Applying \mathbf{G}^{gen} afterward can transform H_{fg} from canonical space to camera space in different timesteps H_{fg}^t . Finally, we combine $\{(H_{\text{fg}}^0, H_{\text{bg}}), (H_{\text{fg}}^1, H_{\text{bg}}), \dots, (H_{\text{fg}}^T, H_{\text{bg}})\}$ and use a renderer (e.g., PyTorch3D [48], Blender [10]) to render the final video. Fig. 3 illustrates the whole inference pipeline.

3.3. Implementation Details

For the stage of learning the species template model, we train for 120 epochs and use a learning rate of $5e^{-4}$ with the AdamW [36] optimizer. For the stage of per-video fine-tuning, we train the NeRF using a learning rate of $1e^{-5}$ with the AdamW optimizer for 120 epochs. For training the motion generator, we use a batch size of 16, a learning rate of $5e^{-4}$, and the Adam [26] optimizer. The weights for the KL-divergence loss are $\lambda_{\mathbf{G}}^{\text{KL}} = 1e^{-2}$, $\lambda_{\mathbf{A}}^{\text{KL}} = 1e^{-4}$, respectively, and the weight for the floating loss is $\lambda_{\text{CDD}} = 0.1$. We adopt data augmentation by applying random rotation and translation for the 3D motion, foreground and background shape. For testing the model in unseen environment meshes, we align the mesh to the same orientation and scale as the training background mesh. For texturing the mesh using SceneTex [6], we use 40 update steps for all prompts. We use PyTorch3D [48] to render the scene when computing FID and Blender [10] to render the meshes.



Diverse Motion Generation

Figure 5. **Diverse Environment-aware Motion Generation.** We show the diverse motion generations in different environments. (Top) We show 4D generation given different starting poses G_0 . (Bottom) We show diverse motion outputs given the same starting pose in the same scene. The proposed method can generate diverse motions in different environments.

4. Experiments

We conduct qualitative and quantitative experiments to evaluate the efficacy of the proposed pipeline. We evaluate the quality and diversity of different methods on a collection of cat videos from RAC [61] and 200 additional collected videos. We also render the 4D generation into videos to evaluate its quality.

Data. For extracting paired 3D motion and environment data, we preprocess each video following RAC [61]. For training the motion generation network, we randomly sample a clip of T frames for each motion sequence extracted from the video. We also translate the background such that its centroid is at the origin $(0, 0, 0)$, and shift the corresponding motion by the same translation. The cat and room meshes for testing are obtained from Turbosquid [1] and 3D-Front [14]. We normalize them with the statistics of the scale and center based on H_{fg} and H_{bg} we obtained from the species-level articulated template shape learning stage.

4.1. Quantitative Evaluation

We evaluate the motion generation model in terms of quality and diversity. We also evaluate the quality of 4D rendering results by testing the model on unseen cat meshes and a novel background mesh.

Metrics. For motion generation, we compute the reconstruction error (Recon.) and the floating error (Floating Err.)

to measure the quality. We compute the L1 distance of the reconstructed trajectory and the ground-truth trajectory for the reconstruction error. To evaluate the floating error, we use the Chamfer distance between the foreground vertices of limb \mathbf{P}_{limb} and the background point-clouds \mathbf{P}_{bg} , excluding the jumping sequence. Chamfer distance is computed by finding the nearest-neighbor matches between points in \mathbf{P}_{limb} and the points in \mathbf{P}_{bg} . For diversity, for each ground-truth trajectory, we generate N motions and compute the L1 distance between the ground-truth and the generated trajectories. For rendering quality, we use Fréchet inception distance (FID) [20] to assess the quality. We compute FID between the rendering of the 4D output generated by our method against the rendering of the ground-truth motion.

Competing Methods. As there are no existing methods for this task, we compare the method against the ablated models – our full model without \mathcal{L}_{CDD} (Ours w/o \mathcal{L}_{CDD}) and without distance feature (Ours w/o D_{fg}).

Results. We show the quantitative result of the motion in Table 1, and the result of the renderings in Table 2. The quality of the proposed method performs favorably against the competing methods while not sacrificing diversity. The diversity of Ours w/o \mathcal{L}_{CDD} is slightly higher than Ours, albeit we observe a much higher Floating Err. This indicates that the diversity comes from generating more floating motions which do not respect the background geometry.

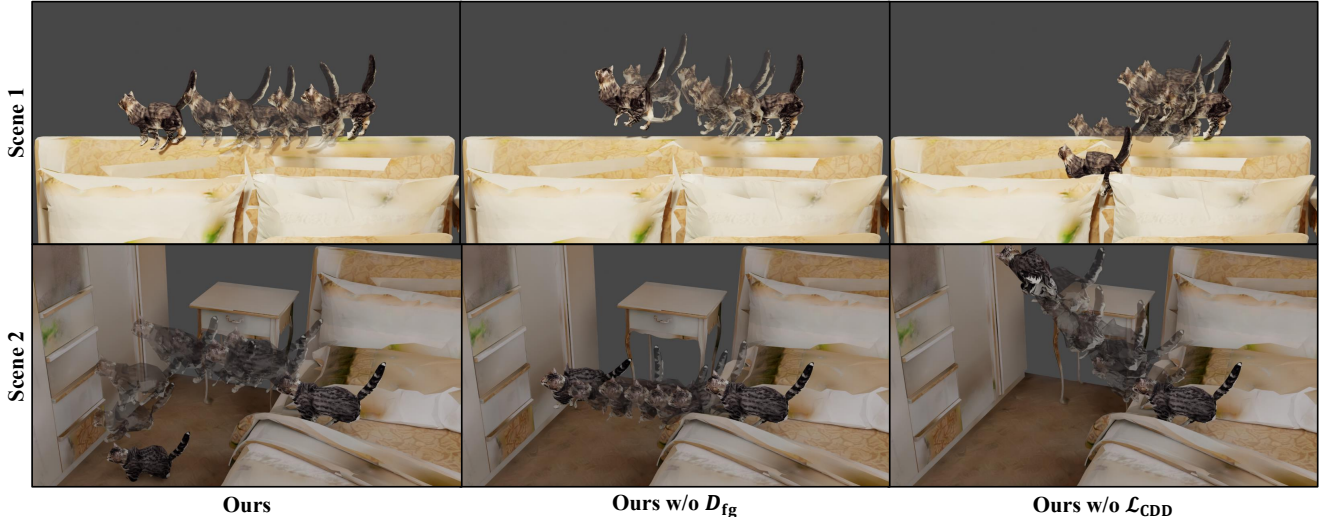


Figure 6. **Ablation analysis.** We ablate the necessity of conditioning on the distance of the foreground mesh center to the background mesh D_{fg} and the floating loss \mathcal{L}_{CDD} . Without D_{fg} and \mathcal{L}_{CDD} , the generated motions cannot faithfully respect the geometry of the 3D scenes and physic constraints.

4.2. Qualitative Evaluation

We show qualitative results of 4D generation and video rendering.

Different Texturing of Foreground and Background.

We show qualitative results of different textured results in Fig. 4. Given a novel mesh of foreground and background, we use Text2tex [7] and different prompts to generate diverse textures for the meshes.

Diverse Rendering of Videos.

We show qualitative results of diverse motion generation in Fig. 5. In the top row, the motion model generates diverse motions by taking a different starting pose G_0 , and it generates diverse motion trajectories such as jumping from table to the sofa, or jumping down to the ground from the table. In the bottom row, the motion model also generates different motions with the same starting pose G_0 and different background H_{bg} as input. For instance, jumping down from the bed or staying in the same position. The rendering results show that the proposed method can generate an environment-aware motion with temporal coherence in the unseen environment.

Comparison with Baseline Methods.

We show a qualitative comparison with competing methods in Fig. 6. Our full model generates the motion sequence which is the most compatible with the background. For example, in Scene 2, the cat in our result jumps down from the bed successfully, while the results of other methods depict a cat that is either moving disregarding scene geometry, or floating unnaturally.

Table 1. **Quantitative evaluation of motion.** We evaluate the trajectory reconstruction ability, motion diversity, floating artifacts.

| Method | Recon. ↓ | Diversity ↑ | Floating Err. ↓ |
|------------------------------|-----------------|-----------------|-----------------|
| Ours w/o \mathcal{L}_{CDD} | 110.5709 | 103.9038 | 45.6105 |
| Ours w/o D_{fg} | 108.1872 | 87.1041 | 43.4656 |
| Ours | 103.4322 | 100.9871 | 38.1343 |

Table 2. **Quantitative evaluation of video rendering.** We evaluate the visual fidelity of the rendered videos.

| Method | FID ↓ |
|------------------------------|-----------------|
| Ours w/o \mathcal{L}_{CDD} | 125.3224 |
| Ours w/o D_{fg} | 126.4011 |
| Ours | 120.4663 |

5. Conclusion and Discussion

We introduce Virtual Pet, a novel framework designed to acquire an environment-aware generative model for 3D motions from a monocular video collection. To extract shape, motion, and affordance from a set of cat videos, we propose a two-stage reconstruction strategy utilizing a combination of a deformable NeRF for articulated 3D reconstruction, and a static NeRF for background scene reconstruction. With the extracted data, we then adopt VAEs to learn to model the motion sequence, consisting of a trajectory generation and articulation generation. The generated motions are environment-aware, incorporating considerations for both foreground and background shapes.

To generate the 4D output, the proposed method operates on a foreground mesh and a background mesh. The generated 4D output can then be rendered into videos given a camera pose and a renderer.

Despite the achieved promising results, our current pipeline also has limitations. First, as the research of 4D reconstruction is still in the early stage, the quality of reconstructed motions has room for improvement. Also, the limited robustness imposes constraints on the filtering of available videos. Second, some generated motions deviate from physical rules, such as gravity. Third, the model is currently species-specific.

For future work, we aim to model finer details of the appearance and the motion. For instance, the fur for different species of the cat, and how it affects the motion. We also leave controllability of the output to future work, such as controlling the cat with natural language. Furthermore, we envision augmenting our training data source with designed 3D assets as well as 2D prior knowledge from large-scale text-to-image models.

Acknowledgements. Work supported in part by NSF grants 2008387, 2045586, 2106825, MRI 1725729, and NIFA award 2020-67021-32799.

References

- [1] Turbosquid 3d models. <https://www.turbosquid.com/>. 7
- [2] Chaitanya Ahuja and Louis-Philippe Morency. Language2pose: Natural language grounded pose forecasting. In *3DV*, 2019. 2
- [3] Aayush Bansal, Minh Vo, Yaser Sheikh, Deva Ramanan, and Srinivasa Narasimhan. 4d visualization of dynamic events from unconstrained multi-view videos. In *CVPR*, 2020. 2
- [4] Emad Barsoum, John Kender, and Zicheng Liu. Hp-gan: Probabilistic 3d human motion prediction via gan. In *CVPRW*, 2018. 2
- [5] Minjie Cai, Kris M Kitani, and Yoichi Sato. Understanding hand-object manipulation with grasp types and object attributes. In *Robotics: Science and Systems*, 2016. 2
- [6] Dave Zhenyu Chen, Haoxuan Li, Hsin-Ying Lee, Sergey Tulyakov, and Matthias Nießner. Scenetex: High-quality texture synthesis for indoor scenes via diffusion priors. *arXiv preprint arXiv:2311.17261*, 2023. 2, 5, 6
- [7] Dave Zhenyu Chen, Yawar Siddiqui, Hsin-Ying Lee, Sergey Tulyakov, and Matthias Nießner. Text2tex: Text-driven texture synthesis via diffusion models. In *ICCV*, 2023. 1, 2, 5, 6, 8
- [8] Rui Chen, Yongwei Chen, Ningxin Jiao, and Kui Jia. Fantasia3d: Disentangling geometry and appearance for high-quality text-to-3d content creation. In *ICCV*, pages 22246–22256, 2023. 1, 2
- [9] Yen-Chi Cheng, Hsin-Ying Lee, Sergey Tulyakov, Alexander G Schwing, and Liang-Yan Gui. Sdfusion: Multimodal 3d shape completion, reconstruction, and generation. In *CVPR*, 2023. 1
- [10] Blender Online Community. *Blender - a 3D modelling and rendering package*. Blender Foundation, Stichting Blender Foundation, Amsterdam, 2018. 6
- [11] Kuan Fang, Te-Lin Wu, Daniel Yang, Silvio Savarese, and Joseph J Lim. Demo2vec: Reasoning object affordances from online videos. In *CVPR*, 2018. 2
- [12] David F Fouhey, Vincent Delaitre, Abhinav Gupta, Alexei A Efros, Ivan Laptev, and Josef Sivic. People watching: Human actions as a cue for single view geometry. In *ECCV*, 2012. 2
- [13] Katerina Fragkiadaki, Sergey Levine, Panna Felsen, and Jitendra Malik. Recurrent network models for human dynamics. In *ICCV*, 2015. 2
- [14] Huan Fu, Bowen Cai, Lin Gao, Ling-Xiao Zhang, Jiaming Wang, Cao Li, Qixun Zeng, Chengyue Sun, Rongfei Jia, Bin-qiang Zhao, et al. 3d-front: 3d furnished rooms with layouts and semantics. In *ICCV*, 2021. 7
- [15] Jun Gao, Tianchang Shen, Zian Wang, Wenzheng Chen, Kangxue Yin, Daiqing Li, Or Litany, Zan Gojcic, and Sanja Fidler. Get3d: A generative model of high quality 3d textured shapes learned from images. *NeurIPS*, 35:31841–31854, 2022. 1
- [16] Chuan Guo, Xinxin Zuo, Sen Wang, Shihao Zou, Qingyao Sun, Annan Deng, Minglun Gong, and Li Cheng. Action2motion: Conditioned generation of 3d human motions. In *ACM MM*, 2020. 2
- [17] Abhinav Gupta, Scott Satkin, Alexei A Efros, and Martial Hebert. From 3d scene geometry to human workspace. In *CVPR*, 2011. 2
- [18] Mohamed Hassan, Vasileios Choutas, Dimitrios Tzionas, and Michael J Black. Resolving 3d human pose ambiguities with 3d scene constraints. In *ICCV*, 2019. 2
- [19] Tucker Hermans, James M Rehg, and Aaron Bobick. Affordance prediction via learned object attributes. In *ICRA*, 2011. 2
- [20] Martin Heusel, Hubert Ramsauer, Thomas Unterthiner, Bernhard Nessler, and Sepp Hochreiter. Gans trained by a two time-scale update rule converge to a local nash equilibrium. *NeurIPS*, 2017. 7
- [21] Chun-Hao P Huang, Hongwei Yi, Markus Höschle, Matvey Safroshkin, Tsvetelina Alexiadis, Senya Polikovsky, Daniel Scharstein, and Michael J Black. Capturing and inferring dense full-body human-scene contact. In *CVPR*, 2022. 2
- [22] Yifei Huang, Minjie Cai, Zhenqiang Li, and Yoichi Sato. Predicting gaze in egocentric video by learning task-dependent attention transition. In *ECCV*, 2018. 2
- [23] Ashesh Jain, Amir R Zamir, Silvio Savarese, and Ashutosh Saxena. Structural-rnn: Deep learning on spatio-temporal graphs. In *CVPR*, 2016. 2
- [24] Yanqin Jiang, Li Zhang, Jin Gao, Weimin Hu, and Yao Yao. Consistent4d: Consistent 360 {deg} dynamic object generation from monocular video. *arXiv preprint arXiv:2311.02848*, 2023. 2
- [25] Ladislav Kavan, Steven Collins, Jiří Žára, and Carol O’Sullivan. Skinning with dual quaternions. In *Proceedings of the 2007 symposium on Interactive 3D graphics and games*, pages 39–46, 2007. 4
- [26] D. P. Kingma and J. Ba. Adam: A Method for Stochastic Optimization. In *ICLR*, 2015. 6
- [27] Hsin-Ying Lee, Xiaodong Yang, Ming-Yu Liu, Ting-Chun Wang, Yu-Ding Lu, Ming-Hsuan Yang, and Jan Kautz. Dancing to music. *NeurIPS*, 2019. 2
- [28] Andreas M Lehrmann, Peter V Gehler, and Sebastian Nowozin. Efficient nonlinear markov models for human motion. In *CVPR*, 2014. 2
- [29] Ruilong Li, Shan Yang, David A Ross, and Angjoo Kanazawa. Ai choreographer: Music conditioned 3d dance generation with aist++. In *ICCV*, 2021. 2
- [30] Tianye Li, Mira Slavcheva, Michael Zollhoefer, Simon Green, Christoph Lassner, Changil Kim, Tanner Schmidt, Steven Lovegrove, Michael Goesele, Richard Newcombe, et al. Neural 3d video synthesis from multi-view video. In *CVPR*, 2022. 1, 2
- [31] Xueting Li, Sifei Liu, Kihwan Kim, Xiaolong Wang, Ming-Hsuan Yang, and Jan Kautz. Putting humans in a scene: Learning affordance in 3d indoor environments. In *CVPR*, 2019. 2
- [32] Zhengqi Li, Simon Niklaus, Noah Snavely, and Oliver Wang. Neural scene flow fields for space-time view synthesis of dynamic scenes. In *CVPR*, 2021. 2
- [33] Chen-Hsuan Lin, Jun Gao, Luming Tang, Towaki Takikawa, Xiaohui Zeng, Xun Huang, Karsten Kreis, Sanja Fidler, Ming-Yu Liu, and Tsung-Yi Lin. Magic3d: High-resolution text-to-3d content creation. In *CVPR*, 2023. 1, 2

- [34] Shaowei Liu, Subarna Tripathi, Somdeb Majumdar, and Xiaolong Wang. Joint hand motion and interaction hotspots prediction from egocentric videos. In *CVPR*, 2022. 2
- [35] William E Lorensen and Harvey E Cline. Marching cubes: A high resolution 3d surface construction algorithm. In *Seminal graphics: pioneering efforts that shaped the field*, 1998. 4
- [36] Ilya Loshchilov and Frank Hutter. Decoupled weight decay regularization. *arXiv preprint arXiv:1711.05101*, 2017. 6
- [37] Julieta Martinez, Michael J Black, and Javier Romero. On human motion prediction using recurrent neural networks. In *CVPR*, 2017. 2
- [38] Ben Mildenhall, Pratul P. Srinivasan, Matthew Tancik, Jonathan T. Barron, Ravi Ramamoorthi, and Ren Ng. Nerf: Representing scenes as neural radiance fields for view synthesis. In *ECCV*, 2020. 2, 3
- [39] Paritosh Mittal, Yen-Chi Cheng, Maneesh Singh, and Shubham Tulsiani. Autosdf: Shape priors for 3d completion, reconstruction and generation. In *CVPR*, 2022. 1
- [40] Tushar Nagarajan, Christoph Feichtenhofer, and Kristen Grauman. Grounded human-object interaction hotspots from video. In *ICCV*, 2019. 2
- [41] Tushar Nagarajan, Yanghao Li, Christoph Feichtenhofer, and Kristen Grauman. Ego-topo: Environment affordances from egocentric video. In *CVPR*, 2020. 2
- [42] Keunhong Park, Utkarsh Sinha, Jonathan T Barron, Sofien Bouaziz, Dan B Goldman, Steven M Seitz, and Ricardo Martin-Brualla. Nerfies: Deformable neural radiance fields. In *ICCV*, 2021. 1, 2
- [43] Keunhong Park, Utkarsh Sinha, Peter Hedman, Jonathan T. Barron, Sofien Bouaziz, Dan B Goldman, Ricardo Martin-Brualla, and Steven M. Seitz. Hypernerf: A higher-dimensional representation for topologically varying neural radiance fields. *ACM TOG*, 2021. 1, 2
- [44] Mathis Petrovich, Michael J Black, and Gül Varol. Action-conditioned 3d human motion synthesis with transformer vae. In *ICCV*, 2021. 2
- [45] Ben Poole, Ajay Jain, Jonathan T Barron, and Ben Mildenhall. Dreamfusion: Text-to-3d using 2d diffusion. *ICLR*, 2022. 1, 2
- [46] Charles R Qi, Hao Su, Kaichun Mo, and Leonidas J Guibas. Pointnet: Deep learning on point sets for 3d classification and segmentation. In *CVPR*, 2017. 5
- [47] Guocheng Qian, Jinjie Mai, Abdullah Hamdi, Jian Ren, Aliaksandr Siarohin, Bing Li, Hsin-Ying Lee, Ivan Skokhodov, Peter Wonka, Sergey Tulyakov, et al. Magic123: One image to high-quality 3d object generation using both 2d and 3d diffusion priors. *arXiv preprint arXiv:2306.17843*, 2023. 1, 2
- [48] Nikhila Ravi, Jeremy Reizenstein, David Novotny, Taylor Gordon, Wan-Yen Lo, Justin Johnson, and Georgia Gkioxari. Accelerating 3d deep learning with pytorch3d. *arXiv:2007.08501*, 2020. 6
- [49] Elad Richardson, Gal Metzger, Yuval Alaluf, Raja Giryes, and Daniel Cohen-Or. Texture: Text-guided texturing of 3d shapes. *arXiv preprint arXiv:2302.01721*, 2023. 1
- [50] Johannes Lutz Schönberger and Jan-Michael Frahm. Structure-from-motion revisited. In *CVPR*, 2016. 2
- [51] Johannes Lutz Schönberger, Enliang Zheng, Marc Pollefeys, and Jan-Michael Frahm. Pixelwise view selection for unstructured multi-view stereo. In *ECCV*, 2016. 2
- [52] Uriel Singer, Shelly Sheynin, Adam Polyak, Oron Ashual, Iurii Makarov, Filippos Kokkinos, Naman Goyal, Andrea Vedaldi, Devi Parikh, Justin Johnson, et al. Text-to-4d dynamic scene generation. *arXiv preprint arXiv:2301.11280*, 2023. 1, 2
- [53] Guy Tevet, Sigal Raab, Brian Gordon, Yonatan Shafir, Daniel Cohen-Or, and Amit H Bermano. Human motion diffusion model. *arXiv preprint arXiv:2209.14916*, 2022. 2
- [54] Liao Wang, Jiakai Zhang, Xinhang Liu, Fuqiang Zhao, Yan-shun Zhang, Yingliang Zhang, Minye Wu, Jingyi Yu, and Lan Xu. Fourier plenotrees for dynamic radiance field rendering in real-time. In *CVPR*, 2022. 2
- [55] Zhengyi Wang, Cheng Lu, Yikai Wang, Fan Bao, Chongxuan Li, Hang Su, and Jun Zhu. Prolificdreamer: High-fidelity and diverse text-to-3d generation with variational score distillation. *arXiv preprint arXiv:2305.16213*, 2023. 1, 2
- [56] Shangzhe Wu, Tomas Jakab, Christian Rupprecht, and Andrea Vedaldi. Dove: Learning deformable 3d objects by watching videos. *IJCV*, 2023. 2
- [57] Wenqi Xian, Jia-Bin Huang, Johannes Kopf, and Changil Kim. Space-time neural irradiance fields for free-viewpoint video. In *CVPR*, 2021. 2
- [58] Gengshan Yang, Deqing Sun, Varun Jampani, Daniel Vlasic, Forrester Cole, Huiwen Chang, Deva Ramanan, William T Freeman, and Ce Liu. Lasr: Learning articulated shape reconstruction from a monocular video. In *CVPR*, 2021. 2
- [59] Gengshan Yang, Deqing Sun, Varun Jampani, Daniel Vlasic, Forrester Cole, Ce Liu, and Deva Ramanan. Viser: Video-specific surface embeddings for articulated 3d shape reconstruction. *NeurIPS*, 2021.
- [60] Gengshan Yang, Minh Vo, Natalia Neverova, Deva Ramanan, Andrea Vedaldi, and Hanbyul Joo. Banmo: Building animatable 3d neural models from many casual videos. In *CVPR*, 2022. 4
- [61] Gengshan Yang, Chaoyang Wang, N Dinesh Reddy, and Deva Ramanan. Reconstructing animatable categories from videos. In *Proceedings of the IEEE/CVF Conference on Computer Vision and Pattern Recognition*, pages 16995–17005, 2023. 1, 2, 3, 4, 7
- [62] Lior Yariv, Jiatao Gu, Yoni Kasten, and Yaron Lipman. Volume rendering of neural implicit surfaces. *NeurIPS*, 2021. 4
- [63] Yufei Ye, Xueting Li, Abhinav Gupta, Shalini De Mello, Stan Birchfield, Jiaming Song, Shubham Tulsiani, and Sifei Liu. Affordance diffusion: Synthesizing hand-object interactions. In *CVPR*, 2023. 2
- [64] Biao Zhang, Matthias Nießner, and Peter Wonka. 3dilig: Irregular latent grids for 3d generative modeling. *NeurIPS*, 2022. 1
- [65] Jiakai Zhang, Xinhang Liu, Xinyi Ye, Fuqiang Zhao, Yan-shun Zhang, Minye Wu, Yingliang Zhang, Lan Xu, and Jingyi Yu. Editable free-viewpoint video using a layered neural representation. *ACM TOG*, 2021. 2

- [66] Siwei Zhang, Yan Zhang, Qianli Ma, Michael J Black, and Siyu Tang. Place: Proximity learning of articulation and contact in 3d environments. In *3DV*. IEEE, 2020. [2](#)
- [67] Yan Zhang, Mohamed Hassan, Heiko Neumann, Michael J Black, and Siyu Tang. Generating 3d people in scenes without people. In *CVPR*, 2020. [2](#)
- [68] Kaifeng Zhao, Shaofei Wang, Yan Zhang, Thabo Beeler, and Siyu Tang. Compositional human-scene interaction synthesis with semantic control. In *ECCV*, 2022. [2](#)
- [69] Joseph Zhu and Peiye Zhuang. Hifa: High-fidelity text-to-3d with advanced diffusion guidance. *arXiv preprint arXiv:2305.18766*, 2023. [2](#)